AIAA'83

AIAA-83-0574

Linear Theory of Pressure Oscillations in Liquid-Fueled Ramjet Engines

V. Yang and F.E.C. Culick, Caltech, Pasadena, CA

AIAA 21st Aerospace Sciences Meeting

January 10-13, 1983/Reno, Nevada

LINEAR THEORY OF PRESSURE OSCILLATIONS IN LIQUID-FUELED RAMJET ENGINES

V. Yang* and F. E. C. Culick**
California Institute of Technology
Pasadena, California

ABSTRACT

Pressure oscillations in ramjet engines are studied within quasi one-dimensional linear acoustics. The flow field in the dump combustor is approximated by division into three parts: a flow of reactants, a region containing combustion products, and a recirculation zone, separated by a flame sheet and a dividing streamline. The three zones are matched by considering kinematic and conservation relations. Acoustic fields in the inlet section and in the combustion chamber are coupled to provide an analytical equation for the complex wave number characterizing the linear stability. The calculated results are compared with the experimental data reported by the Naval Weapons Center. Reasonable agreements are obtained.

I. INTRODUCTION

Suppression of pressure oscillations is a fundamental problem in the design of high performance ramjet engines. Disturbances of this type, generically called combustion instabilities, are a consequence of the sensitivity of combustion processes to local pressure and velocity fluctuations. For low frequency pressure oscillations, this sensitivity is mainly associated with fluid dynamic processes, rather than chemical kinetics. Recent investigation of the low frequency pressure oscillations in ramjet engines[1-7] prompted the work discussed in this paper.

The basic ramjet configuration illustrated in Figure 1 includes a shock wave system at the entrance, an inlet diffuser, a dump combustor, and an exhaust nozzle. Air is delivered to the dump combustor where fuel is injected and burned in the presence of a flame stabilizer. The combustion processes in the dump combustor is extremely complicated, involving turbulent mixing, flame propagation, shear layer, recirculating flow, and finite-rate chemical kinetics. Attempts to model these complicated phenomena have been made for over three decades, but still remain poorly understood. Most of the past work concentrated on investigation of the mean flow fields in the combustor; information available on the treatment of the unsteady flow fields is limited. An excellent review paper concerning the computer modeling of the steady combustion in ramjet combustor has been given by Lilley.[8]

Combustion instabilities in ramjet engines may usually be characterized by several well-defined frequencies. These are close to the frequencies of the natural acoustic modes for the internal cavity of the system. For convenience the oscillatory behavior is classified as bulk, longitudinal, and transverse modes according to the frequency range and spacial structure. Rogers and Marble[9] carried out experiments on screeching instabilities, the relatively high frequency oscillations involving transverse modes, in a two-dimensional ramjet combustor. They found that in the presence of screech, vortices were shed at the flame attachment points, distorting the flame front as they were swept downstream. A mechanism for the screeching oscillations in the ramjet combustor was proposed, based upon transient combustion in the vortices.

For contemporary liquid-fueled ramjets, the most serious problem seems to be low frequency instabilities closely related to longitudinal modes. A very important consequence is the loss of inlet stability margin due to the effect on the inlet shock system. Experimental investigation of this subject has been recently conducted by several research organizations. The results obtained have provided information about the the effects of combustor configuration, fuel type, and fuel-to-air ratio on the overall instability processes. Jarosinski and Wojcicki[10] considered the low frequency combustion instability in a dump combustior which is connected upstream to an acoustic resonator. Shadowgraphs and motion pictures were taken, and measurements were made of the pressure, velocity and local chemi-ionization. They concluded that the combustion instability of this type is closely related to the instability of laminar flames although the combustion processes are distributed over.

Rogers[2] summarized the features of the pressure oscillations in two liquid-fueled engines having very different geometrical configurations. One had an axial dump with a single inlet, and the other had two inlets with a side dump arrangement. Significant differences

---

* Graduate Student

** Professor of Engineering, Associate Fellow, AIAA

appear in the structure of the oscillations excited in the combustion chamber. Schadow and coworkers have studied[5-7] oscillations in a research dump combustor with special attention focused on the inlet shock/acoustic wave interaction. The entire device was extensively instrumented during testing. Two kinds of data have been taken under various operational conditions: the acoustic wave structure and the properties of the inlet shock.

So far as analysis of longitudinal pressure oscillations in ramjets is concerned, Culick and Rogers[3] have constructed an one dimensional linear acoustic model. The combustion processes were accommodated in a general fashion, but not treated in detail. As examples, data were discussed for the two liquid-fueled engines mentioned above. Later, they studied[4] frequency response of a normal shock to downstream disturbances in an inlet diffuser. Two limits of a linearized analysis were discussed; one represented isentropic flows on both sides of a shock wave, and the other might be a crude approximation to the influence of flow separation induced by the wave.

Because observations of the unsteady behavior suggest that the low frequency oscillations do not involve significant transverse motions anywhere in the engine, the analysis here is based on a quasi one-dimensional model. The engine is treated in three parts: the inlet section, the combustion zone, and the region containing combustion products. Each region is handled separately and then matched with adjacent regions. In Section II we discuss the acoustic field in the inlet section. The unsteady motion of the shock wave is characterized by an acoustic admittance function, providing the necessary upstream boundary condition. The acoustic field in the inlet is represented by the superposition of two simple waves running downstream and upstream.

In Section III an integral scheme is developed to study the flow fields in the combustion zone. It is our intention to develop a suitable simple and realistic model accommodating the fundamental features of the flow field, including the flame front, the shear layer, and the recirculating flow. For low frequency oscillations, the flame front and the shear layer can be adequately represented by a flame sheet and an infinitesimally thin vortex sheet, or dividing streamline, respectively. The flow field is, accordingly, decomposed into a flow of reactants, a region containing combustion products, and a recirculation zone, as shown in Figure 1. The three zones are then matched at the flame sheet and the dividing streamline by taking into account conservation and kinematic relations. Determination of their shapes is part of the solution. The unsteady flow fields are considered within linear acoustics and approximated as quasi one-dimensional motion in each region.

Section IV deals with the acoustic field in the completely burned region. Physically, this region ranges from the end of the flame sheet to the entrance of the exhaust nozzle. The mathematical treament of this region is similar to its counterpart in the inlet section except the representation of the exit boundary condition by an admittance function for a compact nozzle.

In Section V the acoustic fields in the three main different regions are matched to provide an analytic equation for the complex wave number which characterizes the linear acoustic field in the entire engine. Calculated results are then compared with experimental data obtained by Schadow et al.[5,7] Good agreement suggests that the model is a satisfactory representation of some of the global behavior of the device.

II. ACOUSTIC FIELD IN THE INLET

The analysis given in this section is identical to that in Reference 4. We ignore the cross-sectional area changes and assume the mean flow field to be uniform. The acoustic field is therefore the superposition of two simple plane waves. One is driven by the pressure oscillations in the combustor and propagates upstream, and the other is reflected by the shock and propagates downstream. Appropriate equations governing the corresponding fields are

$$p_1^{(1)} = [P_1^+ e^{iK_1 x} + P_1^- e^{-iK_1 x}]\, e^{-i(\Omega t + M_1^{(0)} K_1 x)} \tag{2.1a}$$

$$u_1^{(1)} = \frac{1}{\rho_1^{(0)} a_1^{(0)}} [P_1^+ e^{iK_1 x} - P_1^- e^{-iK_1 x}]\, e^{-i(\Omega t + M_1^{(0)} K_1 x)} \tag{2.1b}$$

where the superscripts (0) and (1) represent the mean and the acoustic quantities respectively, Ω is the complex frequency, P_1^+ and P_1^- are complex amplitudes of the right and the left running waves, and K_1 is defined as

$$K_1 = \frac{k_1}{1-M_1^{(0)2}} = \frac{\Omega / a_1^{(0)}}{1-M_1^{(0)2}} = \frac{(\omega + i\alpha)/a_1^{(0)}}{1-M_1^{(0)2}} \tag{2.2}$$

Note that the wave number is complex, the imaginary part being nonzero because of losses in the system. Since this is a linear problem, the wave amplitude can be arbitrarily specified without violating the governing equations. For convenience P_1^+ and P_1^- are chosen to be β and unity respectively. Thus (2.1a) and (2.1b) become

$$p_1^{(1)} = [\beta e^{iK_1 x} + e^{-iK_1 x}]\, e^{-i(\Omega t + M_1^{(0)} K_1 x)} \tag{2.3a}$$

$$u_1^{(1)} = \frac{1}{\rho_1^{(0)} a_1^{(0)}} [\beta e^{iK_1 x} - e^{-iK_1 x}] e^{-i(\Omega t + M_1^{(0)} K_1 x)} \qquad (2.3b)$$

β physically represents the acoustic reflection coefficient at the shock and can be determined by the shock admittance function.

$$\beta = \frac{1 + A_s}{1 - A_s} e^{2iK_1 L_1} \qquad (2.4)$$

By rearranging (2.3a), the acoustic pressure is further expressed in terms of its amplitude and phase.

$$p_1^{(1)} = P_1 e^{-i(\Omega t + M_1^{(0)} K_1 x - \psi_p)} \qquad (2.5)$$

where

$$P_1 = [1 + |\beta|^2 + 2|\beta| \cos(2K_1 x + \varphi)]^{\frac{1}{2}} \qquad (2.6a)$$

$$\psi_p = \tan^{-1}\left[\frac{-\sin K_1 x + |\beta| \sin(K_1 x + \varphi)}{\cos K_1 x + |\beta| \cos(K_1 x + \varphi)}\right] \qquad (2.6b)$$

,and φ is the phase of the reflection coefficient β. It is clear that the acoustic field depends only on the admittance function for the shock wave, the Mach number of the flow, and the complex wave number because any viscous losses in the inlet have been ignored. The calculation of the complex wave number will be described in detail later.

To check the validity of this simple analysis and the shock admittance function derived in Reference 4, a series of numerical comparison with the experimental results obtained at the Naval Weapens Center[7] were conducted, using the measured frequencies of oscillations as known conditions. The shock admittance functions were calculated for two different flow conditions immeadiately behind the shock, isentropic and separated flows according to Culick and Rogers.[4] It was found that the isentropic flow case predicted the result generally well although the latter seemed to serve as a closer approximation to the real problem. Figure 2 shows a typical comparison of the calculated and the measured phase distributions. The phase varies almost linearly because of the small acoustic reflection coefficient at the shock β. A good approximation is given by $(M_1^{(0)}+1)K_1 x$, as easily proven by (2.5) and (2.6b). Figure 3 illustrates the acoustic pressure distributions at various times within one cycle of oscillation. The presence of the extremes on the envelope of the pressure amplitude indicates that the wave is standing, rather than travelling. Each pressure node moves around its mean position periodically, no fixed node point being observed. The same conclusion was reached experimentally by Schadow and his co-researchers.[7]

III. Flow Field in the Combustion Zone

In this section, the steady and unsteady combustion processes in a two-dimensional dump combustor are discussed. The flow field is first approximated by division into two parts: the unburned and the burned regions, separated by a flame sheet, as shown in Figure 4. The flame sheet is an idealized treatment of the combustion processes. It is a surface of discontinuity on which the chemical reactions and rapid state variations take place. Although the flame sheet model serves as an effective tool in the analysis of laminar flame propagation, application to turbulent flames is at best a crude approximation. Only those flows with turbulent scales much greater than flame thickness permit this application,[11] a case not relevant here. As far as the computation of the low frequency unsteady flow fields with flame propagations is concerned, the representation of the flame front by a thin sheet is justified since the sensitivity of combustion processes is mainly associated with fluid dynamic processes, rather than chemical kinetics, and the ratio of the oscillation wavelength to the flame thickness is large.

The sudden change in the cross sectional area of the engine at the dump plane produces recirculating flows which are bounded by shear layers. The density and the temperature fields of the recirculating flow are very close to those of the direct burned flow, but the mean velocity and the mean pressure fields are greatly different.[12] There are strong reversing flows and nonuniformities of the pressure distributions in the recirculation zone. Thus, it is convenient to treat the recirculating flow and the direct burned flow separately. These two regions are separated by a dividing stream surface, or dividing streamline for two-dimensional flow. The shear layer is approximated by a dividing streamline which is essentially treated as a surface of tangential velocity discontinuity. Nevertheless, the model is expected to be valid when the acoustic wave length is long compared with the shear layer thickness.[13] For low frequency oscillations this criterion is met.

If we neglect viscous effects, the flow field in each region can be described by the following equations of continuity and momentum.

$$\frac{\partial \rho}{\partial t} + \frac{\partial}{\partial x}\rho u + \frac{\partial}{\partial y}\rho v = 0 \qquad (3.1)$$

$$\frac{\partial}{\partial t}\rho u + \frac{\partial}{\partial x}\rho u^2 + \frac{\partial}{\partial y}\rho uv + \frac{\partial p}{\partial x} = 0 \qquad (3.2)$$

$$\frac{\partial}{\partial t}\rho v + \frac{\partial}{\partial x}\rho uv + \frac{\partial}{\partial y}\rho v^2 + \frac{\partial p}{\partial y} = 0 \qquad (3.3)$$

Since combustion is confined to the flame sheet, there is no mechanism producing entropy outside the sheet.

The entropy is preserved following fluid elements in each region. As a result, the energy equation can be written in the form

$$\frac{Ds}{Dt} = 0 \tag{3.4}$$

III.1. Matching Conditions

The unburned and the direct burned flows are matched at the flame sheet by using conservation and kinematic relations. They are identical to those derived by Markstein[14] in his study of general problems of unsteady flame propagation. For two-dimensional flow, the kinematic relations are

$$\frac{\partial \eta_1}{\partial t} + u_1(x,\eta_1,t)\frac{\partial \eta_1}{\partial x} = v_1(x,\eta_1,t) - W_1\sec\theta \tag{3.5}$$

$$\frac{\partial \eta_1}{\partial t} + u_2(x,\eta_1,t)\frac{\partial \eta_1}{\partial x} = v_2(x,\eta_1,t) - W_2\sec\theta \tag{3.6}$$

where W_1 and W_2 are the normal flow velocities relative to the flame sheet on the upstream and downstream sides, and η_1 is the y-coordinate of the flame sheet. Note that η_1 depends on both time and space, taking into account the unsteady motion of the flame sheet. For steady motions, (3.5) and (3.6) contain no time-dependent terms and can be derived simply by considering the geometric relations among the flow velocities at the flame sheet.

Conservation laws are applied by considering the flow quantities relative to the flame sheet. The conservations of mass and momentum give

$$\rho_1 W_1 = \rho_2 W_2 \tag{3.7}$$

$$\rho_1 W_1^2 + p_1 = \rho_2 W_2^2 + p_2 \tag{3.8}$$

Since the pressure is continuous along the flame sheet, the tangential velocity component is preserved:

$$u_1(x,\eta_1,t)\cos\theta - v_1(x,\eta_1,t)\sin\theta = u_2(x,\eta_1,t)\cos\theta - v_2(x,\eta_1,t)\sin\theta \tag{3.9}$$

For most cases the changes in the kinetic energy and the pressure across the flame sheet may be ignored in comparison with the heat of combustion, ΔH. Hence, energy conservation requires

$$C_{p1}T_1 + \Delta H = C_{p2}T_2 \tag{3.10}$$

Rearrangement of the above equation for a perfect gas leads to

$$\frac{\rho_1}{\rho_2} = \left[1 + \frac{\Delta H}{C_{p1}T_1}\right]\frac{p_2}{p_1} \tag{3.11}$$

Equation (3.8) implies that the ratio of p_2 to p_1 is of order of the square of the Mach number based upon the flame speed. Thus, it is satisfactory to neglect the pressure change in (3.11).

$$\nu \equiv \frac{\rho_1}{\rho_2} = 1 + \frac{\Delta H}{C_{p1}T_1} \tag{3.12}$$

Physically, the density jump due to the combustion produces volume sources along the flame sheet; their unsteady behaviors are partly responsible for the pressure oscillations in the chamber.

Kinematic relations at the dividing streamline are obtained by considering its instantaneous motion. The results are

$$\frac{\partial \eta_2}{\partial t} + u_2(x,\eta_2,t)\frac{\partial \eta_2}{\partial x} = v_2(x,\eta_2,t) \tag{3.13}$$

$$\frac{\partial \eta_2}{\partial t} + u_3(x,\eta_2,t)\frac{\partial \eta_2}{\partial x} = v_3(x,\eta_2,t) \tag{3.14}$$

Because the dividing streamline is a streamline across which there is no flow but the tangential velocity is discontinuous, the only relation available is the continuity of pressure:

$$p_2(x,\eta_2,t) = p_3(x,\eta_2,t) \tag{3.15}$$

The flame speed W_1 is required to complete the matching conditions. It is modeled according to the simple formula proposed by Thurston[15] in his experimental investigation of two-dimensional flames stabilized by bluff body flame holders.

$$W_1 = \chi V_1 \approx \chi u_1(x,\eta_1,t) \tag{3.16}$$

where V_1 is the velocity of the upstream flow and χ is an empirical parameter depending on the properties of the combustible mixture.

III.2. Integral Equations

To formulate the flow field in terms of integrated variables, we first integrate the continuity equation for the unburned flow in the region I. The procedure is similar to that employed by Marble and Candel[24] in their study of two-dimensional flame propagations.

$$\int_0^{\eta_1}\frac{\partial \rho_1}{\partial t}dy + \int_0^{\eta_1}\frac{\partial}{\partial x}\rho_1 u_1 dy + \int_0^{\eta_1}\frac{\partial}{\partial x}\rho_1 v_1 dy = 0$$

Integration by parts with η_1 a function of axial position and time gives

$$\frac{\partial}{\partial t}\int_0^{\eta_1}\rho_1 dy + \frac{\partial}{\partial x}\int_0^{\eta_1}\rho_1 u_1 dy - \rho_1 u_1(x,\eta_1,t)\frac{\partial \eta_1}{\partial x} - \rho_1\frac{\partial \eta_1}{\partial t} + \rho_1 v_1(x,\eta_1,t) - \rho_1 v_1(x,0,t) = 0$$

Application of the kinematic relation (3.5) at the flame sheet and consideration of the symmetry about the axis give the final result for the equation for

conservation of mass in region I:

$$\frac{\partial}{\partial t}\int_0^{\eta_1}\rho_1 dy + \frac{\partial}{\partial x}\int_0^{\eta_1}\rho_1 u_1 dy + \rho_1 W_1 \sec\theta = 0 \qquad (3.17)$$

A similar integration of the other conservation equations results in the following integral equations. momentum equation (region I)

$$\frac{\partial}{\partial t}\int_0^{\eta_1}\rho_1 u_1 dy + \frac{\partial}{\partial x}\int_0^{\eta_1}\rho_1 u_1^2 dy + \int_0^{\eta_1}\frac{\partial p_1}{\partial x}dy$$

$$+ \rho_1 u_1(x,\eta_1,t) W_1 \sec\theta = 0 \qquad (3.18)$$

mass equation (region II)

$$\frac{\partial}{\partial t}\int_{\eta_1}^{\eta_2}\rho_2 dy + \frac{\partial}{\partial x}\int_{\eta_1}^{\eta_2}\rho_2 u_2 dy - \rho_2 W_2 \sec\theta = 0 \qquad (3.19)$$

momentum equation (region II)

$$\frac{\partial}{\partial t}\int_{\eta_1}^{\eta_2}\rho_2 u_2 dy + \frac{\partial}{\partial x}\int_{\eta_1}^{\eta_2}\rho_2 u_2^2 dy + \int_{\eta_1}^{\eta_2}\frac{\partial p_2}{\partial x}dy$$

$$- \rho_2 u_2(x,\eta_1,t) W_2 \sec\theta = 0 \qquad (3.20)$$

mass equation (region III)

$$\frac{\partial}{\partial t}\int_{\eta_2}^{R}\rho_3 dy + \frac{\partial}{\partial x}\int_{\eta_2}^{R}\rho_3 u_3 dy = 0 \qquad (3.21)$$

momentum equation (region III)

$$\frac{\partial}{\partial t}\int_{\eta_2}^{R}\rho_3 u_3 dy + \frac{\partial}{\partial x}\int_{\eta_2}^{R}\rho_3 u_3^2 dy + \int_{\eta_2}^{R}\frac{\partial p_3}{\partial x}dy = 0 \qquad (3.22)$$

The dependent variables are written as sums of mean and fluctuating quantities. region I

$$\rho_1(x,y,t) = \rho_1^{(0)} + \rho_1^{(1)}(x,t) \qquad (3.23a)$$

$$u_1(x,y,t) = u_1^{(0)}(x,y) + u_1^{(1)}(x,t) \qquad (3.23b)$$

$$p_1(x,t) = p_1^{(0)}(x) + p_1^{(1)}(x,t) \qquad (3.23c)$$

region II

$$\rho_2(x,y,t) = \rho_2^{(0)} + \rho_2^{(1)}(x,t) \qquad (3.23d)$$

$$u_2(x,y,t) = u_2^{(0)}(x,y) + u_2^{(1)}(x,t) \qquad (3.23e)$$

$$p_2(x,t) = p_2^{(0)}(x) + p_2^{(1)}(x,t) \qquad (3.23f)$$

region III

$$\rho_3(x,y,t) = \rho_2^{(0)} + \rho_3^{(1)}(x,t) \qquad (3.23g)$$

$$u_3(x,y,t) = u_3^{(0)}(x,y) + u_3^{(1)}(x,t) \qquad (3.23h)$$

$$p_3(x,y,t) = p_3^{(0)}(x,y) + p_3^{(1)}(x,t) \qquad (3.23i)$$

Thus, we treat a two-dimensional mean flow field with a quasi one-dimensional unsteady flow field. Because the radii of curvature of streamlines are large except in the recirculation zone, the equation of motion in the vertical direction assures that the variations of pressure across regions 1 and 2 are negligible. Consequently, the mean pressures in regions 1 and 2 are assumed to be functions of x only. In this work, we do not make the strictly one-dimensional assumptions for the acoustic fields, i,e.,

$$u_1^{(1)}(x,t) = u_2^{(1)}(x,t) = u_3^{(1)}(x,t), \text{ etc.}$$

It may serve as the first approximation to the problem.

The present model has two advantanges. First, the difference between the acoustic characteristics of the unburned and burned flows is taken into account. Second, the unsteady motions of the flame sheet and the dividing streamline as well as their effects on the acoustic field can be accommodated.

III.3. Mean Flow Fields in the Combustion Zone

The mean flow field must be known for analysis of the unsteady motions. We consider the mean recirculating flow first. The recirculation zone is treated as a closed region bounded by a dividing streamline. Because the inner boundary layer thickness is small in comparison with the width of the recirculation zone and the viscous and turbulent stresses decay rapidly away from the shear layer, the so-called frozen vorticity theory[16] is used. The vorticity distribution is assumed to be uniform, the diffusion of vorticity due to viscosity and turbulence being ignored. The representation of the recirculating flow by a flow of constant vorticity with slip at the boundary has been found to be adequate. For example, Smith[17] considered such representation for the flow in the region of the trailing edge of an aerofoil. Taulbee and Robertson[18] used it to study the turbulent separation bubble ahead of a step. Fairlie[19] applied this model to two-dimensional separation bubbles. The model provided good agreement with experiments in all cases. Thus, we use the following equation of motion for the mean recirculating flow.

$$\nabla^2\psi = -\omega_0, \ \psi = 0 \text{ along the boundary} \qquad (3.24)$$

The stream function is ψ and ω_0 is the constant vorticity, treated here as an empirical constant to be specified. The mean velocity field is obtained from the definition of the stream function.

$$u_3^{(0)}(x,y) = \frac{\partial\psi}{\partial y}, \ v_3^{(0)}(x,y) = -\frac{\partial\psi}{\partial x} \qquad (3.25)$$

Consequently, the mean pressure field can be calculated since the total pressure is preserved along each streamline.

$$p_3^{(0)} + \frac{1}{2}\rho_2^{(0)} V_3^{(0)2} = \text{constant} \qquad (3.26)$$

The integral conservation equations for the mean flow fields in regions I and II are obtained by considering the time invariant part of (3.17-20). Thus, we have steady mass equation (region I)

$$\frac{d}{dx}[\bar{u}_1^{(0)}\eta_1^{(0)}] + W_1\sec\theta^{(0)} = 0 \tag{3.27}$$

steady momentum equation (region I)

$$\frac{d}{dx}[\bar{u}_1^{(0)2}\eta_1^{(0)}] + \frac{\eta_1^{(0)}}{\rho_1^{(0)}}\frac{dp_1^{(0)}}{dx}$$

$$+ u_1^{(0)}(x,\eta_1^{(0)})W_1\sec\theta^{(0)} = 0 \tag{3.28}$$

steady mass equation (region II)

$$\frac{d}{dx}[\bar{u}_2^{(0)}(\eta_2^{(0)} - \eta_1^{(0)})] - W_2\sec\theta^{(0)} = 0 \tag{3.29}$$

steady momentum equation (region II)

$$\frac{d}{dx}[\bar{u}_2^{(0)2}(\eta_2^{(0)} - \eta_1^{(0)})] + \frac{(\eta_2^{(0)} - \eta_1^{(0)})}{\rho_2^{(0)}}\frac{dp_2^{(0)}}{dx}$$

$$- u_2^{(0)}(x,\eta_1^{(0)})W_2\sec\theta^{(0)} = 0 \tag{3.30}$$

where $\bar{u}_1^{(0)}$ and $\bar{u}_2^{(0)}$ are the average axial velocities defined as

$$\bar{u}_1^{(0)} = \frac{1}{\eta_1^{(0)}}\int_0^{\eta_1^{(0)}} u_1^{(0)}(x,y)dy,$$

$$\bar{u}_2^{(0)} = \frac{1}{\eta_2^{(0)} - \eta_1^{(0)}}\int_{\eta_1^{(0)}}^{\eta_2^{(0)}} u_2^{(0)}(x,y)dy$$

In the derivation of (3.27-30), the following two conventional assumptions were made, similar to those used in the shallow water wave calculations.

$$\int_0^{\eta_1^{(0)}} [u_1^{(0)}(x,y) - \bar{u}_1^{(0)}]^2dy = 0,$$

$$\int_{\eta_1^{(0)}}^{\eta_2^{(0)}} [u_2^{(0)}(x,y) - \bar{u}_2^{(0)}]^2dy = 0,$$

Notice that the momentum integral equations explicitly involve the local velocity components at the flame sheet, $u_1^{(0)}(x,\eta_1^{(0)})$ and $u_2^{(0)}(x,\eta_1^{(0)})$. To complete the theoretical formulation, they must be determined in terms of the flame height $\eta_1^{(0)}$ and the integrated flow variables. The following remarks describe a simple independent analysis of the flow field in region I, providing the necessary information.

Since the flow upstream of the flame sheet is inviscid and irrotational, the velocity potential satisfies the Laplace equation.

$$\nabla^2\varphi = 0, \tag{3.31}$$

subject to the proper boundary conditions. Solution of the above equation may be written in the following form.

$$\varphi = Ux + \sum_{m=1}^{m=\infty} A_m e^{\frac{m\pi}{r}x}\cos(\frac{m\pi}{r}y) \tag{3.32}$$

where U is the inlet flow velocity and A_m's are constants to be calculated from the boundary conditions at the flame sheet. As a first approximation we shall account for the first term in the series only. This term is assumed to represent the general characteristics of the unburned flow to a sufficiently good approxiation.[20] Thus, an equation relating the local velocities at the flame sheet is obtained from (3.32):

$$\frac{v_1^{(0)}(x,\eta_1^{(0)})}{u_1^{(0)}(x,\eta_1^{(0)}) - U} = -\tan(\frac{\pi}{r}\eta_1^{(0)}) \tag{3.33}$$

Combination of (3.33) with (3.5), (3.6), and (3.9) gives the expressions for $u_1^{(0)}(x,\eta_1^{(0)})$ and $u_2^{(0)}(x,\eta_1^{(0)})$.

$$u_1^{(0)}(x,\eta_1^{(0)}) = \frac{U\tan(\frac{\pi}{r}\eta_1^{(0)}) - W_1\sec\theta^{(0)}}{\frac{d\eta_1^{(0)}}{dx} + \tan(\frac{\pi}{r}\eta_1^{(0)})} \tag{3.34}$$

$$u_2^{(0)}(x,\eta_1^{(0)}) = \frac{U\tan(\frac{\pi}{r}\eta_1^{(0)}) - W_1\sec\theta^{(0)}}{\frac{d\eta_1^{(0)}}{dx} + \tan(\frac{\pi}{r}\eta_1^{(0)})}$$

$$+ W_1(\nu - 1)\sin\theta^{(0)} \tag{3.35}$$

Hence, the theoretical model for the mean flow fields is completed by substituting the above two equations into the integral momentum equations.

The overall calculation using the integral scheme based upon iteration procedures proceeds as follows. We first assume a dividing streamline shape and solve the Poisson equation (3.24) and (3.25) numerically for the velocity field in the recirculation. A standard five point scheme is used to formulate the finite difference equations which are then solved by the successive over relaxation (SOR) method.[21] The pressure distribution along the dividing streamline is calculated according to the Bernoulli equation (3.26). With the result available as a known condition, the integral scheme governing the flow fields in the unburned and the direct burned regions is carried out to the end of the recirculation zone. Determination of the shapes of the dividing streamline and flame sheet is part of the solution obtained. Another calculation of the recirculating flow continues, using the new dividing streamline shape, and the whole procedure is repeated. The iterative computation halts when the solutions become convergent, the changes in the dividing streamline shape from step to step being small. The integral scheme is then performed to the end of the flame sheet to

complete the solution.

Numerical calculations have been done for the mean flow fields in a reserach dump combustor operated at the Naval Weapens Center[5]. The data characterizing a typical experiment is given in Table 1.

Table 1. Computer program input variables

u_{in}=190 m/s	p_{in}=561774 N/m^2
ρ_{in}=4.1 Kg/m^3	ω_0=2500 1/s
T_{in}=477 K	a_{in}=438 m/s
d=0.0635 m	h=0.03175 m
L_1=0.762 m	L_2=0.762 m
ν=4	χ=0.05

Figure 5 summarizes the various distributions in the unburned flow. Upstream of the reattachment point, the pressure variation, dominated by the recirculating flow, is small; the effect of combustion appears in the determination of the flame and the dividing streamline shapes. For positions downstream the combustion plays a decisive role. As a consequence of the influence of combustion on the axial pressure gradient, the flow becomes accelerated, rapid velocity increase taking place. A kink, corresponding to the reattachment point, is observed on the flame sheet. The slope of the flame sheet gradually decreases near the kink, then grows after that point. This can be interpreted by appeal to the momentum balance. Because the pressure gradient tends to be small in the reattaching region, the flame shape must become flatter in order to reduce the momentum influx into the burned flow region. This phenomenon has also been found experimentally in the Caltech experiments.[22]

Figure 6 shows the shapes of the dividing streamline for different cases. These shapes are dominated primarily by the flame speed and the ratio of the unburned to the burned gas density although the vortex strength plays an important role in determining the velocity field in the recirculating zone. Because of the small radius of curvature of the dividing streamline caused by high vorticity, the length of the recirculation zone decreases as the vorticity ω_0 increases. The influences of the flame speed and the density ratio on the dividing streamline shape can be interpretd in terms of the momentum balance. The higher flame speed, or the higher density ratio, usually implies the greater momentum influx into the direct burned region where the pressure field is mostly determined by the recirculating flow. For a given vortex strength this in turn produces a steeper dividing streamline to balance the momentum. Figure 7 illustrates the dependence of the flame shape on various parameters.

In the development of the integral scheme, we encountered a closure problem, which was then solved by proposing a simple independent equation (3.33) to formulate of the local flow velocities at the flame sheet. A similar issue was found by Subbaiah[23] in his study of the non-steady behavior of a flame stabilized by a flame holder at the center of a two-dimensional duct. He carried out a more thorough analysis of the irrotational flow field upstream of the flame to provide the sufficient conditions for the completeness of the model. In order to check the validity of the present work, specifically equation (3.33), we apply our model to the problem dealt with in Reference 23 and use exactly the same input parameters. For this comparison, the recirculating flow immediately behind the flame holder is not accounted for in the computation. Figure 8 shows that the agreement is resonably good.

III.4. Unsteady Flow Fields in the Combustion Zone

The unsteady flow field in the combustion zone is formulated by considering the time-dependent counterpart to the steady analysis of the integral relations. It is treated within quasi one-dimensional linear acoustics. With the proposed decompositions of the flow variables and consideration of the first order terms only, the mass integral equation for the unburned flow in region I becomes

$$\frac{\partial}{\partial t}\left[\int_0^{\eta_1^{(0)}} \rho_1^{(1)} dy + \int_{\eta_1^{(0)}}^{\eta_1^{(0)}+\eta_1^{(1)}} \rho_1^{(0)} dy\right] +$$

$$\frac{\partial}{\partial x}\left[\int_0^{\eta_1^{(0)}} (\rho_1^{(0)} u_1^{(1)} + \rho_1^{(1)} u_1^{(0)}) dy + \int_{\eta_1^{(0)}}^{\eta_1^{(0)}+\eta_1^{(1)}} \rho_1^{(0)} u_1^{(0)} dy\right]$$

$$+ \rho_1^{(1)} W_1 \sec\theta^{(0)} - \rho_1^{(0)} W_1 \frac{\sin\theta^{(0)}}{\cos^2\theta^{(0)}} \frac{\partial \eta_1^{(1)}}{\partial x} = 0$$

Rearrangement of the above equation yields

$$\frac{\partial}{\partial t}\left[\rho_1^{(0)}\eta_1^{(1)} + \rho_1^{(1)}\eta_1^{(0)}\right] + \frac{\partial}{\partial x}\left[\rho_1^{(0)} u_1^{(0)}(x,\eta_1^{(0)})\eta_1^{(1)}\right.$$

$$\left. + \rho_1^{(1)} u_1^{(0)}\eta_1^{(0)} + \rho_1^{(0)} u_1^{(1)}\eta_1^{(0)}\right]$$

$$+ \rho_1^{(1)} W_1 \sec\theta^{(0)} - \rho_1^{(0)} W_1 \frac{\sin\theta^{(0)}}{\cos^2\theta^{(0)}} \frac{\partial \eta_1^{(1)}}{\partial x} = 0 \qquad (3.36)$$

Similar manipulations of the other integral formulas produce a system of equations governing the unsteady flow field.

Because the pressure across the dividing streamline is continuous,

$$p_2^{(1)}(x,t) = p_3^{(1)}(x,t) \qquad (3.37)$$

The acoustic velocity may be discontinuous across the unsteady shear layer modeled as a surface of tangential velocity discontinuity. Treating the problem in this way, we have crudely included the effect of the shear layer on the acoustic field. As mentioned earlier, there

is no entropy-producing mechanism away from the flame sheet. The flow is isentropic in the unburned and the burned flow regions respectively. As a result, the acoustic density field can be related to its pressure field through the isentropic relation.

$$\rho_1^{(1)} = p_1^{(1)}/a_1^{(0)2}, \quad \rho_2^{(1)} = p_2^{(1)}/a_2^{(0)2} \tag{3.38}$$

Thus, the formulation for the linear acoustic fields is completed. In summary, there are six integral equations for six unknowns $u_1^{(1)}$, $u_2^{(1)}$, $u_3^{(1)}$, $\eta_1^{(1)}$, $\eta_2^{(1)}$, and $p_1^{(1)}$. Note that $p_2^{(1)}$ is related to $p_1^{(1)}$ through the momentum balance across the flame sheet (3.8).

For convenience the governing equations are put in their matrix form.

$$A_1(x)\frac{\partial q(x,t)}{\partial t} + A_2(x)\frac{\partial q(x,t)}{\partial x} = A_3(x)q(x,t) \tag{3.39}$$

where $A_1(x)$, $A_2(x)$, and $A_3(x)$ are coefficient matrices containing the information about the mean flow fields, and $q(x,t)$ is a vector for the unsteady flow variables. For harmonic motions, the time-dependent and the spatial-dependent parts of each variable are separated.

$$q(x,t) = \hat{q}(x)e^{-i\Omega t} \tag{3.40}$$

where Ω is the complex freqency. Substitution of (3.40) into (3.39) and rearrangement of the result produce a system of ordinary differential equations with complex coefficients.

$$\frac{d\hat{q}(x)}{dx} = [i\Omega B(x) + C(x)]\hat{q}(x) \tag{3.41}$$

where $B(x)=A_2(x)^{-1}A_1(x)$ and $C(x)=A_2(x)^{-1}A_3(x)$. $A_2(x)$ is regular except at three singular points, the flame attachment point, the shear layer reattachment point, and the end of the flame zone. Mathematically, (3.41) represents a two-point boundary value problem with the eigenvalue Ω. The specification of the boundary conditions at the dump plane and the end of the flame sheet will be discussed later.

A series expansion method is used to solve (3.41) for the complex eigenvalue Ω because of its computational efficiency and simplicity. We expand the coefficient matrices and the flow variable vector in powers of x,

$$B(x)=\sum_{m=1}^{\infty} B_m x^m,\ C(x)=\sum_{m=1}^{\infty} C_m x^m,\ \hat{q}(x)=\sum_{m=1}^{\infty} \hat{q}_m x^m \tag{3.42}$$

where B_m and C_m are constant matrices, and $\hat{q}_m$ is a constant vector. Substitution of the above expansions into (3.41) and collection of coefficients of equal powers of x yield

$$\hat{q}_m = \frac{1}{m}\sum_{j=0}^{m-1}(i\Omega B_j + C_j)\hat{q}_{(m-1-j)} \tag{3.43}$$

subject to the boundary conditions,

$$\hat{q}(0) = \hat{q}_0 \text{ and } \hat{q}(L) = \sum_{m=0}^{\infty}\hat{q}_m L^m \tag{3.44}$$

The whole problem is solved by first specifying $\hat{q}_0$ from the boundary condition at the dump plane (x=0). As a result, the constant vectors $\hat{q}_m$'s (m=1,2,...) are determined by carrying out (3.43). Application of another boundary condition at the end of the flame sheet (x=L) produces a transcendental equation for Ω.

Before dealing with the complicated ramjet problems, it may be helpful to give a simple example demonstrating the validity of this technique. Consider a two-point boundary value problem as follows.

$u'' + \lambda^2 u = 0$, with $u(0)=0$, $u(1)=0$

The exact solution for the eigenvalue is $m\pi$ (m=1,2,...). The series expansion method with M terms retained yields the approximated solutions shown in Table 2.

Table 2. Calculated eigenvalues

M = 5	% error
λ_1 = 3.141148	$1.4\ 10^{-2}$
M = 7	% error
λ_1 = 3.141592	$1.9\ 10^{-5}$
λ_2 = 6.416062	$2.0\ 10^{-0}$
M = 9	% error
λ_1 = 3.141593	$1.9\ 10^{-5}$
λ_2 = 6.284237	$1.7\ 10^{-2}$

Clearly, the method functions well; the solution converges rapidly, especially for the lower modes.

IV. ACOUSTIC FIELD DOWNSTREAM OF THE COMBUSTION ZONE

Physically, this region contains the completely burned gas flow, ranging from the end of the flame sheet (x=L) to the entrance of the exhaust nozzle ($x=L_2$). The nozzle is assumed to be acoustic compact and characterized by an acoustic admittance function. The mathematical treatment of the acoustic field in this region is similar to that in the inlet section except for the different mean flow field and boundary conditions. Again, the field contains two simple waves; the acoustic pressure and velocity are

$$p_2^{(1)}=[P_2^+e^{iK_2x}+P_2^-e^{-iK_2x}]e^{-i(\Omega t+M_2^{(0)}K_2x)} \tag{4.1a}$$

$$u_2^{(1)}=\frac{1}{\rho_2^{(0)}a_2^{(0)}}[P_2^+e^{iK_2x}-P_2^-e^{-iK_2x}]e^{-i(\Omega t+M_2^{(0)}K_2x)} \qquad (4.1b)$$

where P_2^+ and P_2^- are the complex wave amplitudes and K_2 is defined as

$$K_2=\frac{k_2}{1-M_2^{(0)2}}=\frac{\Omega/a_2^{(0)}}{1-M_2^{(0)2}}=\frac{(\omega+i\alpha)/a_2^{(0)}}{1-M_2^{(0)2}} \qquad (4.2)$$

The complex wave numbers K_2 differs from K_1 because the speeds of sound are different in the two regions. Defining the admittance function for the nozzle A_n at $x=L_2$ and rearranging the result, we find the relation between P_2^+ and P_2^-.

$$\frac{P_2^+}{P_2^-}=\frac{1+A_n}{1-A_n}e^{-2iK_2L_2} \qquad (4.3)$$

Substitution of the above equation into (4.1a) and (4.1b) gives

$$p_2^{(1)}=P_2^-[\frac{1+A_n}{1-A_n}e^{iK_2(x-2L_2)}+e^{-iK_2x}]\cdot$$

$$e^{-i(\Omega t+M_2^{(0)}K_2x)} \qquad (4.4a)$$

$$u_2^{(1)}=\frac{P_2^-}{\rho_2^{(0)}a_2^{(0)}}[\frac{1+A_n}{1-A_n}e^{iK_2(x-2L_2)}-e^{-iK_2x}]\cdot$$

$$e^{-i(\Omega t+M_2^{(0)}K_2x)} \qquad (4.4b)$$

Thus, the acoustic field in this region can be determined after the complex wave number and the wave amplitude P_2^- are obtained.

V. ACOUSTIC FIELD IN THE ENTIRE ENGINE

The acoustic field in the combustion zone must be coupled to the fields upstream of the dump plane and downstream of the end of the flame sheet. For linear problems this procedure eventually produces a transcendental equation for the complex wave number characterizing the acoustic field in the entire engine. The coupling is expressed by requiring that the acoustic pressure and mass flux be continuous. Thus, the boundary condition for the unburned flow at the dump plane can be specified from (2.3a) and (2.3b). They are

$$p_1^{(1)}(0,t)=[\beta+1]e^{-i\Omega t} \qquad (5.1)$$

$$u_1^{(1)}(0,t)=\frac{1}{\rho_1^{(0)}a_1^{(0)}}[\beta-1]e^{-i\Omega t} \qquad (5.2)$$

The flame sheet and the dividing streamline are assumed to be attached to the edge of the step.

$$\eta_1^{(1)}(0,t)=0 \text{ and } \eta_2^{(1)}(0,t)=0 \qquad (5.3)$$

Since the perturbation velocities vanish at the rigid wall,

$$u_2^{(1)}(0,t)=0 \text{ and } u_3^{(1)}(0,t)=0 \qquad (5.4)$$

Finally, the time-dependent part of the momentum balance across the flame sheet (3.8) gives the equation for the acoustic pressure of the burned flow at the dump plane.

$$p_2^{(1)}(0,t)=\frac{1+W_1^2/a_1^{(0)2}}{1+W_2^2/a_2^{(0)2}}[\beta+1]e^{-i\Omega t} \qquad (5.5)$$

The matching condition at the end of the flame sheet ($x=L$) are given by (4.4a) and (4.4b).

$$p_2^{(1)}(L,t)=P_2^-[\frac{1+A_n}{1-A_n}e^{iK_2(L-2L_2)}+e^{-iK_2L}]\cdot$$

$$e^{-i(\Omega t+M_2^{(0)}K_2L)} \qquad (5.6a)$$

$$u_2^{(1)}(L,t)=\frac{P_2^-}{\rho_2^{(0)}a_2^{(0)}}[\frac{1+A_n}{1-A_n}e^{iK_2(L-2L_2)}-e^{-iK_2L}]\cdot$$

$$e^{-i(\Omega t+M_2^{(0)}K_2L)} \qquad (5.6b)$$

Because this is a linear problem, the complex wave number must be solved for before the wave amplitude P_2^- can be determined. Hence, the proper boundary condition to be satisfied at $x=L$ is

$$\frac{u_2^{(1)}(L,t)\,(\rho_2^{(0)}a_2^{(0)})}{p_2^{(1)}(L,t)}=\frac{e^{2iK_2(L-L_2)}-1}{e^{2iK_2(L-L_2)}+1} \qquad (5.7)$$

The combination of the integral scheme constructed in Section III.4 and the boundary conditions given above forms a well-posed problem which can be solved for the complex frequency Ω. The computation is based on an iteration procedure and proceeds as follows. A value for the complex frequency is assumed, and the boundary conditions at the dump plane are calculated from (5.1-5). These determine the constant vector $\vec{q}_m$ ($m=1,2,\ldots$) in (3.44), according to (3.43). As a result, the flow variables at $x=L$ are obtained to check the boundary condition. A new procedure is repeated by assuming another complex frequency Ω until (5.7) is satisfied. To improve the rate of convergence of the iterative scheme, we utilize an IMSL routine ZANLYT in which the Muller method with deflation is used.[25]

VI. RESULTS AND DISCUSSION

The calculated frequencies and growth constants of oscillations in a research dump combustor at the Naval Weapens Center for the test conditions given in Table.1 are shown in Table 3.

Table 3. Calculated complex frequencies

first mode	f=280 Hz	α=-60.9 1/s
second mode	f=527 Hz	α=-52.1 1/s
third mode	f=628 Hz	α=-77.4 1/s

The calculated frequency of the second mode checks the measured result (f=540 Hz) well. The growth constant is negative, the wave amplitude decaying with time. This is a consequence of the incomplete representation of the combustion processes. Within the present model, the acoustic energy gained from the combustion processes does not compensate the energy losses at the inlet shock and the exhaust nozzle. Hence, the waves appear to be stable.

Figure 9 shows the comparison of the measured and calculated acoustic pressure distributions. Because the theory is linear, the amplitude distribution contains an arbitrary multiplying constant whose value has been adjusted to provide reasonable comparison with experimental data. The effective wave number in the inlet is greater than that in the combustor roughly by a factor of 1.5 due to the smaller speed of sound. In the combustor, the wave shape is noticeably nonsinusoidal, changing rapidly in the region adjacent to the dump plane. This is caused by the complex effects of the recirculating flow, the shear layer, and the combustion processes on the acoustic wave.

The phase distriution for the acoustic field is shown in Figure 10. As discussed in Section II, the phase distribution in the inlet is almost linear. The acoustic field is driven by the pressure oscillations in the combustion chamber and damped significantly by the shock. A peak corresponding to the shear layer reattachment point is observed on the phase distribution in the combustor. The phase changes approximately 180 degree from the dump plane to that point, and gradually decays after it. Comparison of the phase distributions at other modes, as shown in Figures 11 and 12, shows that the peak appears for all modes.

Figure 11 shows the pressure and the phase distributions for the first mode oscillation. The acoustic field is roughly a bulk mode except for the rapid variation of the phase near the reattachment point. This bulk oscillation has been observed in the same engine under different operational conditions and in some other engines.[2] For the third mode oscillation, the phase distribution illustrated in Figure 12 exhibits a plateau, approximately ranging from the reattachment point to the end of the flame sheet. Significant phase changes occur near those two positions. This phenomenon indicates that for higher mode oscillations the phase distribution is sentitive to the positions of the reattachment point and the end of the flame sheet.

VII. CONCLUSION AND SUMMARY

1. An integral scheme was developed to study the steady and the unsteady flow fields in a two-dimensional dump combustor.
2. A standing wave system, driven by the combustion processes in the dump combustor and damped by the shock, is formed in the inlet.
3. The calculated pressure and phase distributions and frequency of the second mode oscillation check the measured results well.
4. Rapid acoustic pressure and phase changes occur near the shear layer reattachment point, indicating that the unsteady shear layer may play an important role for low frequency oscillations.

ACKNOWLEDGEMENTS

This work was supported by the California Institute of Technology and by the Air Force Office of Scientific Research, Grant No. AFOSR-80-0265.

REFERENCE

[1] Culick, F.E.C., "Report of the JANNAF Workshop on Pressure Oscillations in Ramjets," *1980 JANNAF Propulsion Meeting*, March 1980; *17th JANNAF Combustion Meeting*, September 1980.

[2] Rogers, T., "Pressure Oscillations in Small Ramjet Engines," *16th JANNAF Combustion Meeting*, September 1980.

[3] Culick, F.E.C., and Rogers, T., "Modeling of Pressure Oscillations in Ramjets," *AIAA/SAE/ASME 16th Joint Propulsion Conference*, June 1980.

[4] Culick, F.E.C., and Rogers, T., "The Response of Normal Shocks in Inlet Diffusers," *AIAA/SAE/ASME 17th Joint Propulsion Conference*, July 1981.

[5] Crump, J.E., Schadow, K.C., Blomshield, F., and Bicker, C.J., "Combustion Instability in a Researcher Dump Combustor: Pressure Oscillations," *18th JANNAF Combustion Meeting*, October 1981.

[6] Schadow, K.C., Crump, J.E., and Blomshield, F., "Combustion Instability in a Researcher Dump Combustor: Inlet Shock Oscillations," *18th JANNAF Combustion Meeting*, October 1981.

[7] Crump, J.E., Schadow, K.C., Blomshield, F., Culick, F.E.C., and Yang, V., "Combustion Instability in Dump Combustors: Acoustic Mode Determinations," *19th JANNAF Combustion Meeting*,

November 1982.

[8] Lilley, G.D., "Computer Modeling of Ramjet Combustors," *AIAA Journal*, Vol. **19**, No. 12, 1981, pp. 1562-1563.

[9] Rogers, D.E. and Marbel, F.E., "A Mechanism for High Frequency Oscillations in Ramjet Combustors and Afterburners," *Jet Propulsion*, Vol. **26**, 1956, pp. 456-462.

[10] Jarosinski, J. and Wojcicki, S., "The Mechanism of Interaction between a Combustion Region and Acoustic Resonator," *Acta Astronautica*, Vol. **3**, 1976, pp. 567-572.

[11] Williams, F.A., "A Review of Some Theoretical Considerations of Turbulent Flame Structures," *AGARD-CP-164* 1974, Sec. II-1.

[12] Williams, F.A., *Combustion Theory*, Addison-Wesley Publishing Company, 1965.

[13] Michalke, A., "On the Inviscid Instability of Hyperbolic Tangent Velocity Profile," *Journal of Fluid Mechanics*, Vol. **19**, 1964, pp. 543-556.

[14] Markstein, G.H., *Nonsteady Flame Propagation*, The MacMillan Company, 1964.

[15] Thurston, D.W., "An Experimental Investigation of Flame Spreading from Bluff Body Flameholder," Thesis, California institute of Technology, Pasadena, Californis, 1958.

[16] Batchelor, G.K., "A Proposal Concerning Laminar Wakes behind Bluff Bodies at Large Reynolds Number," *Journal of Fluid Mechanics*, Vol. **1**, 1956, pp. 388-398.

[17] Smith, P.D., "A Note on the Computation of the Inviscis Rotational Flow Past the Trailing Edge of an Aerofoil," *R. A. E. Tech Memo. Aero. 1217.*

[18] Taulbee, D.B. and Robertson, J.M., "Turbulent Separation Analysis Ahead of a Step," *Journal of Basic Engineering*, Vol. **D94**, 1972, pp. 544-550.

[19] Fairlie, B.D., "An Analysis of Separation in Turbulent Boundary Layers," Ph.D. Thesis, University of Melbourne, Melbourne, Australia, 1973.

[20] Zeldovich,Y.B., Istratov, A.G., Kidin, N.I., and Librovich, V.B., "Flame Propagation in Tubes: Hydrodynamics and Stability," *Combustion Science and Technology*, Vol. **24**, 1980, pp. 1-13.

[21] Meis, T., *Numerical Solution of Partial Differential Equations*, Springer-Verlag, New York, 1981.

[22] Smith, D., Private Commutation.

[23] Subbaiah, M.V., "Non-Steady Behavior of Flame Spreading in a Two-Dimensional Duct," *AIAA/SAE/ASME 17th Joint Propulsion Conference*, July 1981.

[24] Marble, F.E. and Candel, S.M., "An Analytical Study of the Non-Steady Behaviour of Large Combustor," *Seventeenth Symposium (International) on Combustion*, August 1978, pp.761-769.

[25] *IMSL Library*, Edition 9, IMSL, Inc., 1982

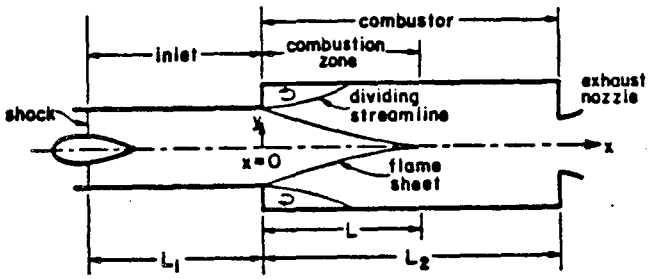

Figure 1. Schematic Diagram of Ramjet Engine

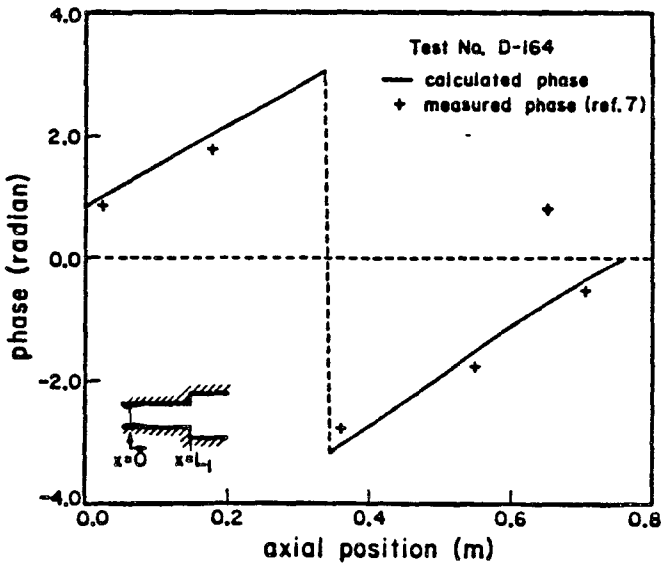

Figure 2. Measured and Calculated Phase Distributions in the Inlet

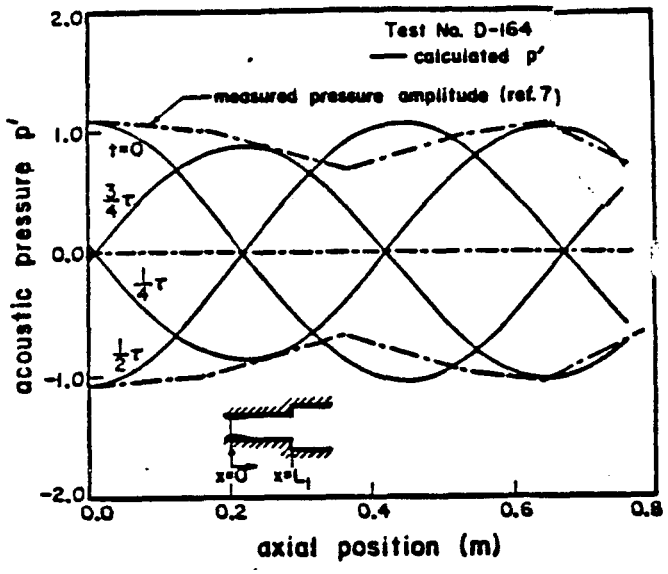

Figure 3. Measured and Calculated Acoustic Pressure Distributions in the Inlet

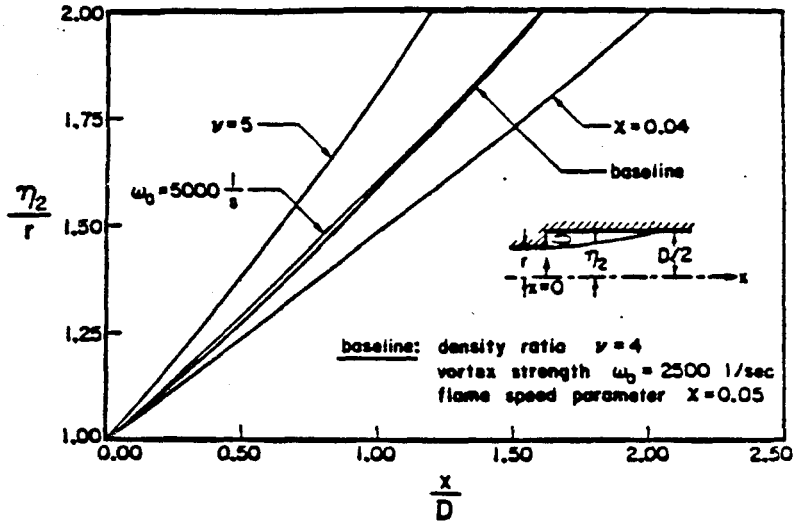

Figure 6. Shapes of Mean Dividing Streamline

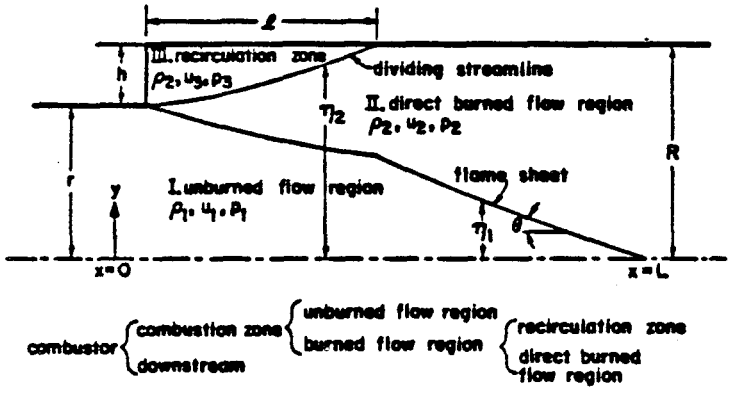

Figure 4. Flow Field in the Two-Dimensional Dump Combustor

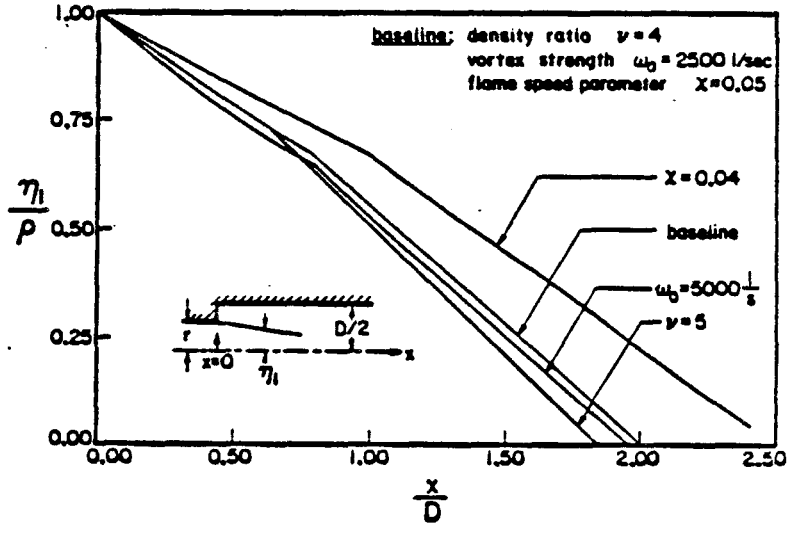

Figure 7. Steady Flame Envelopes

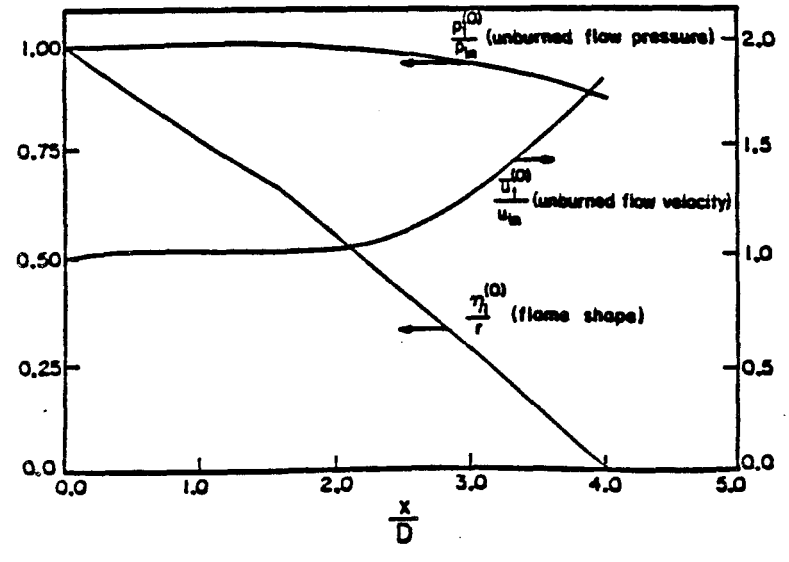

Figure 5. Distributions of Mean Flow Variables

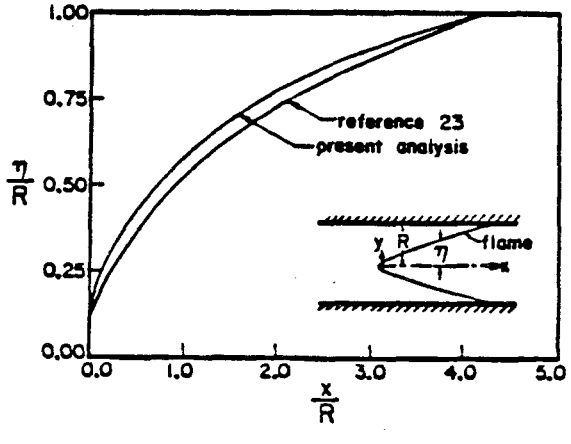

Figure 8. Steady Flame Sheets in a Two-Dimensional Duct

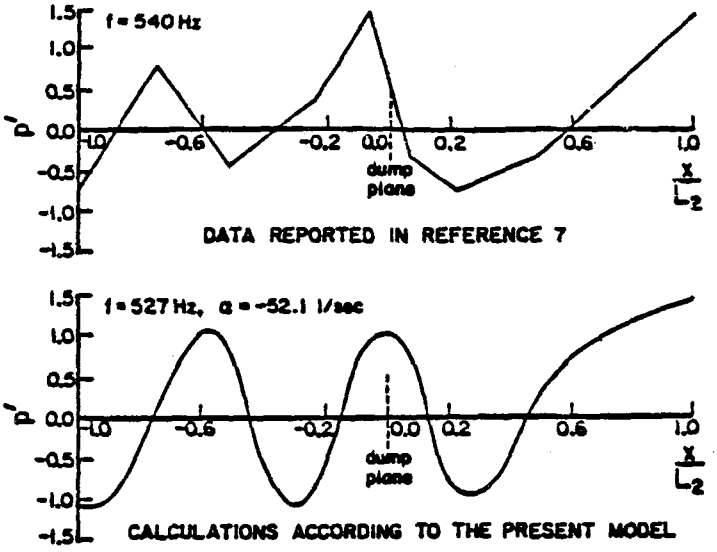

Figure 9. Measured and Calculated Acoustic Pressure Distributions in the Entire Engine

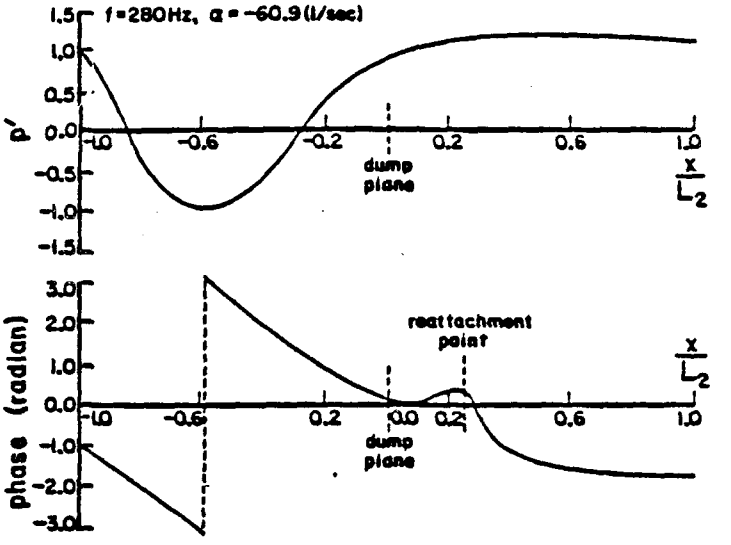

Figure 11. Calculated Acoustic Pressure and Phase Distributions of the First Mode

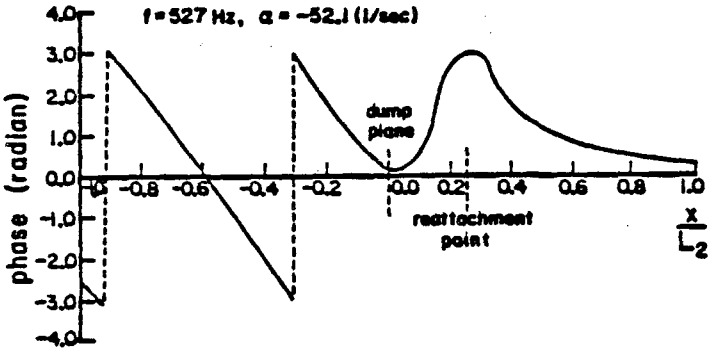

Figure 10. Calculated Phase Distribution of the Second Mode

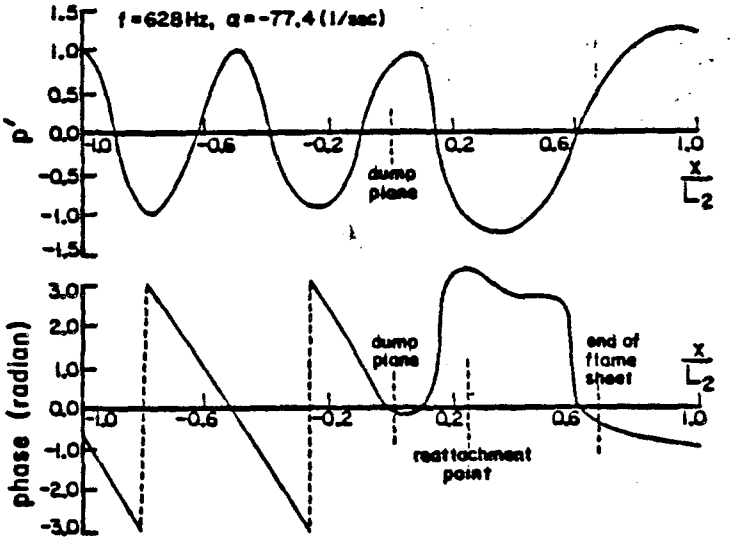

Figure 12. Calculated Acoustic Pressure and Phase Distributions of the Third Mode